PHYSICAL REVIEW B **81**, 081203(R) (2010)

Model of the electrochemical conversion of an undoped organic semiconductor film to a doped conductor film

M. Modestov, V. Bychkov, G. Brodin, D. Valiev, and M. Marklund*
The Plasma and Nonlinear Physics Group, Department of Physics, Umeå University, SE-901 87 Umeå, Sweden

P. Matyba and L. Edman
The Organic Photonics and Electronics Group, Department of Physics, Umeå University, SE-901 87 Umeå, Sweden
(Received 31 December 2009; published 16 February 2010)

We develop a model describing the electrochemical conversion of an organic semiconductor (specifically, the active material in a light-emitting electrochemical cell) from the undoped nonconducting state to the doped conducting state. The model, an extended Nernst-Planck-Poisson model, takes into account both strongly concentration-dependent mobility and diffusion for the electronic charge carriers and the Nernst equation in the doped conducting regions. The standard Nernst-Planck-Poisson model is shown to fail in its description of the properties of the doping front. Solving our extended model numerically, we demonstrate that doping front progression in light-emitting electrochemical cells can be accurately described.

DOI: 10.1103/PhysRevB.81.081203 PACS number(s): 72.10.−d, 82.45.Wx

The pioneering demonstration that it is possible to perform doping on an organic conjugated polymer and attain a high metalliclike electronic conductivity was awarded with the Nobel Prize in Chemistry in 2000.[1] The general opportunity for a controlled tuning of the electronic and optical properties of organic semiconductors via various doping techniques has opened up for a wide range of emerging novel and flexible applications. It also provides for important and stimulating science as regards to the fundamental processes in organic semiconductors, as a number of interesting features of these materials originate in their specific properties and distinguish them from inorganic semiconductors.[2–4] First, electrochemical and chemical doping can be performed with straightforward means *in situ*. By applying an appropriate voltage to an electrode coated with an organic semiconductor film and in contact with an electrolyte, it is possible to inject electronic charge into the organic semiconductor, which subsequently is electrostatically compensated by injection (ejection) of ions from (into) the electrolyte.[5,6] The necessary motion of ions within the organic film is facilitated by its soft, and in some cases porous, nature. Second, the doping levels correlating to a high electronic conductivity is much higher in organic semiconductors than in their inorganic counterparts ($\sim$0.1 vs $\sim 10^{-4}$ dopants/repeat unit), which is a direct consequence of the self-localization effects in organic semiconductors and the concomitant positive dependence of the mobility (μ) of electrons and holes on concentration (n).[4,7,8] Finally, the mobility $\mu(n)$ exhibits a strong dependence on the doping mode, and a much stronger positive dependence is in effect when nearby compensating (and lattice-polarizing) counterions are present, as is the case in electrochemical and chemical doping, than when the electronic charge carriers are introduced in, e.g., a field-effect mode.[4,8] However, current models [see, e.g., the review (Ref. 9) and references therein] of such systems are not able to explain experimental data on the formation of a doping front or the properties of such a front.

In this Rapid Communication, we develop an extended Nernst-Planck-Poisson model describing the electrochemical conversion of an organic semiconductor film from the undoped nonconducting state to the doped conducting state. As compared to the standard Nernst-Planck-Poisson description,[9] our model takes into account both strongly concentration-dependent mobility as well as the Nernst equation in the doped conducting regions. We compare the analytical and numerical results with recently acquired experimental data. It is demonstrated that the observed doping front in light-emitting electrochemical cell (LEC) devices can *only* be described by our extended model, while the standard Nernst-Planck-Poisson model fails in its description. The experimental setup in conjunction with our model thus allows us to draw important conclusion about the general dynamics of the doping process in an organic semiconductor.

A typical LEC consists of a solid-state active material, comprising an intimate blend of a fluorescent conjugated polymer electrolyte positioned between two electrodes. When a voltage equal to or larger than the band-gap potential of the conjugated polymer is applied between the two electrodes ($V \geq E_g/e$), balanced charge injection (electrons at the cathode and holes at the anode) into the conjugated polymer is facilitated by the preceding migratory motion of the electrochemically inert ions and the corresponding formation of electric double layers at the two electrode interfaces. The injected electronic charge carriers are electrostatically neutralized by the compensatory motion of ions in a process termed electrochemical doping; p-type doping (i.e., injection of holes and compensation by anions) takes place at the positive anode and n-type doping (injection of electrons and compensation by cations) at the negative cathode, and after a "turn-on time" a light-emitting p-n junction is formed in the interelectrode gap.[10–15] The doping of a fluorescent conjugated polymer has a "dark" optical signature in that the formation of dopants (polarons) is concomitant with the formation of low-energy sites with limited radiative-decay probability from the excited state (i.e., quenched fluorescence). Figure 1(a) presents a photograph of a planar LEC device during operation at $V=5$ V ($>E_g/e$) and under UV light illumination in a dark room. The anode/cathode is

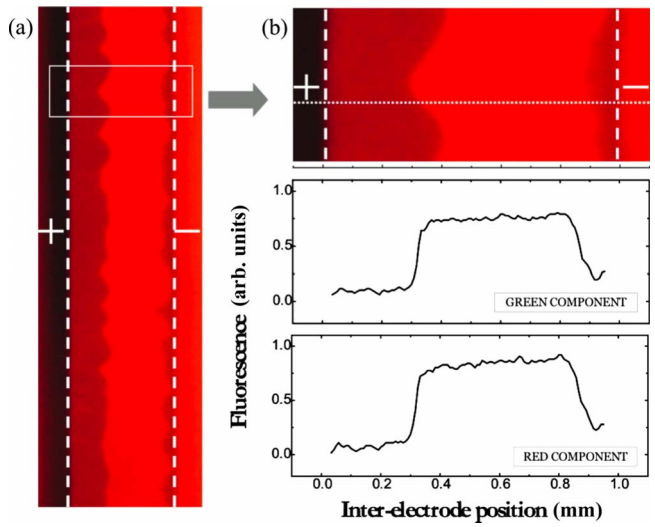

FIG. 1. (Color online) (a) Photograph of a planar Au/{MEH-PPV+PEO+KCF_3SO_3}/Au device with a 1 mm interelectrode gap during operation at $V=5$ V and $T=360$ K. The anode and cathode are indicated by a (+) and a (−) sign, respectively. The device was operated in a dark room under UV illumination, so that the *p*-type and *n*-type doping regions are visualized as dark regions originating from the anodic and cathodic interfaces, respectively. (b) Enlarged section of the photograph in (a), as indicated by the solid line. The dotted line in (b) marks the path in the interelectrode gap along which the fluorescence quenching data of (c) the green component and (d) the red component were extracted from the photograph.

marked with a "+/−." The fluorescence quenching of the "green" and the "red" components of the photograph along a representative path in the interelectrode gap [as indicated by the dotted line in Fig. 1(b)] are presented in Figs. 1(c) and 1(d), respectively. Two observed distinct dark regions with very low fluorescence intensity correspond to *p*-type and *n*-type doping. The regions originate at the anodic and cathodic interfaces and end with a very sharp and rather irregularly shaped front boundary. By correlating the size and growth of each doped region with the temporal evolution of the integrated current, it is possible to extract important information as regards to the doping concentration and profile. We have recently demonstrated that the doping concentration in the doped regions is very high, with a value of the order of $\sim 10^{26}$ dopants/m^3 (corresponding to ~ 0.1 dopants/repeat unit),[16] and that the doping concentration behind the doping front is relatively constant.[17–20]

The organic semiconductor material will be modeled as consisting of electrons and holes together with positive and negative ions in a polymer structure. Diffusion and mobility of charges are of primary importance, which may be studied using the methods of plasma physics. Similar models have been presented before,[9] but we will show that very important aspects have previously been overlooked. In particular, we include an injection barrier in the form of the Nernst potential in conjunction with a concentration-dependent mobility, which are necessary to obtain agreement between theory and experiments. The particle species in the material satisfy the force balance equation

$$nm\dot{\mathbf{v}} = -qn\nabla(\phi - \phi_N) - k_B T \nabla n - \tau^{-1} nm\mathbf{v}, \quad (1)$$

where n denotes the concentration, m is the mass, $\mathbf{v}$ is the velocity, q is the charge, k_B is Boltzmann's constant, T is the temperature, τ is the concentration-dependent time between collisions, and $\phi - \phi_N$ is the *overpotential* experienced by the particle. Here we have introduced a phenomenological injection barrier ϕ_N due to the difference in Fermi levels for the electrons and holes between the doped and undoped regions. Ions do not experience any barrier so that ϕ_N should be set to zero for the ions. In the electrochemical system under study, the injection process is not limiting, i.e., the electronic species on both sides of the barrier are at quasiequilibrium, and ϕ_N is chosen to be the Nernst potential

$$\phi_N(n_{h,e}, T) = (k_B T/q_{h,e}) \ln[n_{h,e}/(n_{h,e,\infty} - n_{h,e})], \quad (2)$$

where $n_{h,e,\infty}$ is the maximum concentration of holes (label "*h*") or electrons (label "*e*"). The Nernst potential originates from quantum effects, and the interpretation of ϕ_N in terms of an electrostatic force should therefore be done with caution. The Nernst potential is valid only in the highly doped region, and it should be set formally to zero in the undoped region, $\phi_N(n_{h,e}, T) = 0$. When going over from one region to another, we match the solutions by fitting the functions and their derivatives.

On the time scales of interest here, i.e., much longer than the collision time τ, the collision force dominates over the particle acceleration $mn\dot{\mathbf{v}}$, such that the left-hand side of Eq. (1) can be neglected. Then $\mathbf{v} = -Dn^{-1}\nabla n \pm \mu\nabla(\phi - \phi_N)$, where the mobility is given by $\mu = \tau|q|/m$, the diffusion coefficient D follows from the Einstein relation $\mu = |q|D/k_B T$ and $\pm$ correspond to positive and negative charges. Substituting $\mathbf{v}$ into the continuity equations for all species we obtain the extended Nernst-Planck-Poisson equations for the semiconductor system

$$\partial_t n_{h,e} - \nabla \cdot [\pm \mu_{h,e} n_{h,e} \nabla(\phi - \phi_N) + D_{h,e} \nabla n_{h,e}] = 0, \quad (3)$$

$$\partial_t n_{\pm} - \nabla \cdot [\pm \mu_{\pm} n_{\pm} \nabla \phi + D_{\pm} \nabla n_{\pm}] = 0. \quad (4)$$

The labels denote holes (h), electrons (e), positive (+) and negative (−) ions. The electrostatic potential ϕ is determined by Poisson's equation $\varepsilon_0 \nabla^2 \phi = -e(n_+ + n_h - n_- - n_e)$. Still, in our system, the quasineutrality condition $n_+ + n_h - n_- - n_e = 0$ is satisfied with very good accuracy. We note that the quasineutrality condition does *not* imply a constant electric-field strength, but rather indicates that small charge imbalance causes extremely large electric fields.[22]

In what follows we will focus on the dynamics and structure of the *p*-type doping, but the analysis could of course equally well be applied to the *n*-type doping. Equations (3) and (4) admit a solution in a form of a localized planar doping front resembling a shock, moving with velocity U and converting the undoped polymer into a doped polymer (for a similar observation in ferroelectric crystals, see Ref. 23). In the undoped region (label 0), we have a uniform electric field $-\partial_x \phi_0$, uniform initial concentration of ions $n_{+0} = n_{-0} \equiv n_0$, and no holes, $n_{h0} = 0$. Behind the front, in the highly *p*-doped region (label ∞), the hole concentration is denoted by $n_{h\infty}$, while the electric field $-\partial_x \phi_\infty$ and ion concentrations $n_{\pm\infty}$ are

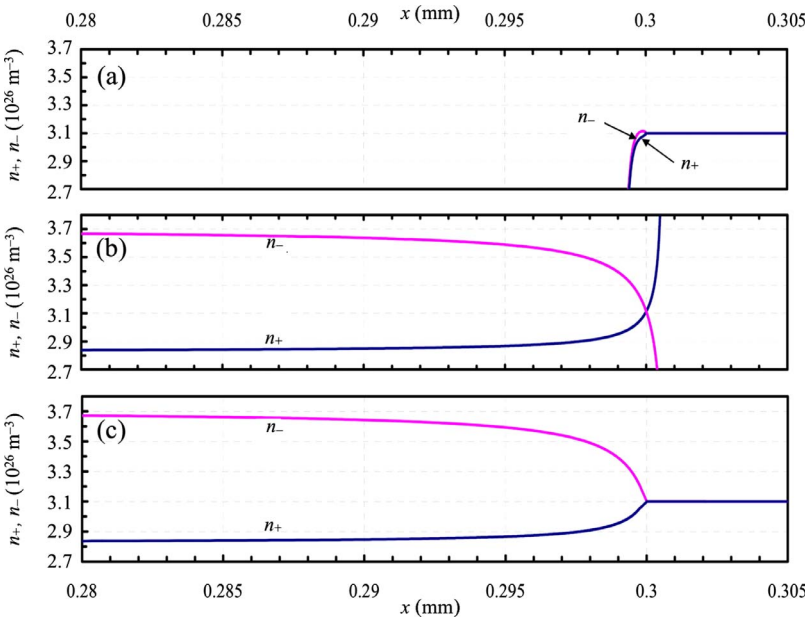

FIG. 2. (Color online) Model data for the concentration of ions as a function of distance from the positive anode, resulting from the employment of: (a) concentration-*dependent* mobility for the electronic charge carriers, (b) concentration-*independent* mobility and the Nernst equation in the doped regions, and (c) concentration-*dependent* mobility and the Nernst equation in the doped region.

obtained from Eq. (3) and the quasineutrality condition. In the reference frame of the doping front ($\partial_t n=0$), we may integrate Eqs. (3) and (4) to obtain

$$D_h \partial_x n_h = -n_h U - n_h \mu_h \partial_x (\phi - \phi_N), \tag{5}$$

$$D_\pm \partial_x n_\pm = (n_0 - n_\pm) U \pm \mu_\pm (n_\pm \partial_x \phi - n_0 \partial_x \phi_0) \tag{6}$$

for the holes and ions, respectively. The electric field in the p-doped region is negligible due to the high mobility of the holes relative the ions. Noting that the concentration gradients vanish on each side of the doping front, we obtain the p-front velocity

$$U = -(n_0/n_{h\infty})(\mu_+ + \mu_-)\partial_x \phi_0. \tag{7}$$

Diffusion does not influence front velocity (7) but instead determines the structure and width of the front.

A dimensional analysis suggests the characteristic width of the front $L_f = D_-/U$. However, L_f does not portray the full structure of the doping front, since there are several different characteristic length scales within the front, from the undoped to the doped region. The hole mobility is highly sensitive to the concentration, and in the undoped region $\mu_{h0}/\mu_\pm \ll 1$. Thus, from Eqs. (5) and (6) we also find that the characteristic length scale in the undoped region is given by $(\mu_{h0}/\mu_\pm)L_f$, which may be orders of magnitude smaller than L_f. As a result, one can expect a sharp head of the doping front with strong concentration gradients. On the other hand, for the doped region, Eqs. (5) and (6) predict a slow variation in the front due to $\mu_{h\infty}/\mu_\pm \gg 1$ and the Nernst potential. The concentration approaches the final value asymptotically according to the power law $(\mu_+/\mu_- + 1)L_f/(x - x_f)$, where $x - x_f$ measures the distance from the leading edge of the doping front. This gives a very smooth behavior of the doping front in the highly conducting part of the polymer. The analytical reasoning has been supported by the numerical solution to Eqs. (5) and (6), described below and presented in Figs. 2 and 3. Thus, the structure of the doping front and the generic features of the doping process are reproduced by our model, both analytically and numerically. Some of the length scales presented above could be measured in future high-resolution experiments.

As stated above, our model makes use of the concentration dependence of the hole mobility (see, e.g., Refs. 7 and 8). In the numerical solution we employ the following empirical concentration-dependent mobility for holes as extracted from Ref. 8

$$\mu_h = 3.85 \times 10^{-8} \left[1 + \tanh\left(26.6 \frac{n_h}{n_0} - 4.3 \right) \right] \ \mathrm{m^2/V\ s}. \tag{8}$$

Note that we have renormalized the mobility data in accordance with data from Ref. 24 to account for the lower mobility of MEH-PPV in comparison to the conjugated polymer under study in Ref. 25. To first approximation the ion mobility does not depend on

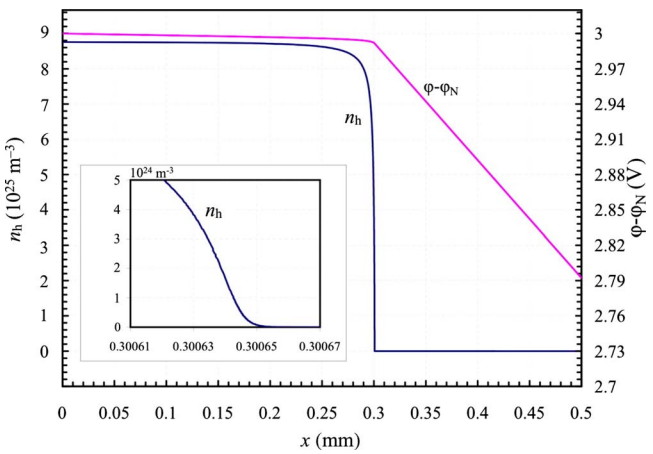

FIG. 3. (Color online) Model data showing concentration of holes, and the overpotential profile as a function of distance from positive electrode.

concentration. To analyze Eqs. (5) and (6) numerically, we use Eq. (8) and empirical data[17,18,25] at the early stage of the doping process: $n_0=3.1\times10^{26}$ m^{-3}, $d\phi_0/dx=3$ V/mm, $\mu_+=1.0\times10^{-10}$ m^2/V s, $\mu_-=2.2\times10^{-10}$ m^2/V s, $n_{h\infty}=8.8\times10^{25}$ m^{-3}, and $T=360$ K. The respective numerical solution is shown in Figs. 2 and 3. Figure 2 shows the ionic concentrations as a function of distance from the anode (x) when the p-type doping front has progressed to $x=0.3$ mm. We note the highly resolved x axis. Our model solution is shown in Fig. 2(c), while Figs. 2(a) and 2(b) illustrate the unphysical results without employing the Nernst equation and concentration-dependent mobility, respectively. First, by omitting the Nernst term, we obtain correct concentrations in the undoped region but cannot achieve physically sound results in the doped region [Fig. 2(a)]. Second, if we instead keep the Nernst term, and assume a constant hole mobility, the doped side of the front is described quite well. However, ionic concentration levels diverge rapidly in the undoped region [Fig. 2(b)]. If we, on the other hand, include both correct concentration-dependent mobility (8) as well as Nernst term (2), we obtain the physically sound result shown in Fig. 2(c). Here we can see the emergence of a doping front that has a shape in good agreement with the experimental observations of Fig. 1. The doping front in Fig. 2(c) has a characteristic width of $\approx0.1-0.2$ mm, a consequence of the long tail due to the Nernst term in Eqs. (6) and (7). At the leading edge of the front, the gradients look very sharp as compared to the trailing edge. This follows from the low hole mobility in the undoped region, and a higher resolution of the leading edge demonstrates that the characteristic length scale is $(\mu_{h0}/\mu_\pm)L_f\approx2\times10^{-4}$ mm, see the insert of Fig. 3. Figure 3 shows the concentration of holes within the front, and the overpotential profile as a function of distance from the anode. Again, in agreement with the previous discussion, we observe a very sharp leading edge of the front and a smooth long tail. The plot demonstrates a weakly varying overpotential at the trailing edge of the front. We also compare quantitatively the theoretical predictions for the doping front velocity and the experimental measurements. Using Eq. (7) and the experimental data we calculate the front velocity at the beginning of the doping process as $U=13.5\times10^{-6}$ m/s. The experimental measurements provided the same initial value for the front velocity, $U=13.5\times10^{-6}$ m/s, within the accuracy of measurements. As the doping progresses, the p- and n-type doping fronts accelerate toward each other,[21] due to the decrease in distance between the fronts.

Thus, our model is in very good agreement with the experiments, both qualitatively and quantitatively. It predicts the quantitative value of the doping front velocity with good accuracy. The model also gives good agreement between the observed and calculated front thickness. Furthermore, it reproduces the correct front structure as a combination of smooth tail and very sharp leading edge. Though the present analysis is one dimensional, it can be easily extended to a multidimensional case. However, the study of multidimensional effects is left for future research.

This work was supported by the Swedish Research Council under the under Contract No. 2007-4422, 2008-4422 and by the Kempe Foundation. L.E. was supported by a grant from the Knut and Alice Wallenberg Foundation.

*mattias.marklund@physics.umu.se

[1] A. J. Heeger, Rev. Mod. Phys. **73**, 681 (2001).
[2] G. Malliaras and R. Friend, Phys. Today **58**(5), 53 (2005).
[3] V. I. Arkhipov, P. Heremans, E. V. Emelianova, and H. Bassler, Phys. Rev. B **71**, 045214 (2005).
[4] V. I. Arkhipov, E. V. Emelianova, P. Heremans, and H. Bassler, Phys. Rev. B **72**, 235202 (2005).
[5] Q. Pei and O. Inganäs, Adv. Mater. **4**, 277 (1992).
[6] J. H. Hou *et al.*, Chem. Commun. (Cambridge) 2008, 6034.
[7] X. Jiang *et al.*, Chem. Phys. Lett. **364**, 616 (2002).
[8] H. Shimotani, G. Diguet, and Y. Iwasa, Appl. Phys. Lett. **86**, 022104 (2005).
[9] R. B. Schoch, J. Han, and P. Renaud, Rev. Mod. Phys. **80**, 839 (2008).
[10] L. Edman, Electrochim. Acta **50**, 3878 (2005).
[11] J. M. Leger, S. A. Carter, and B. Ruhstaller, J. Appl. Phys. **98**, 124907 (2005).
[12] P. Matyba, K. Maturova, M. Kemerink, N. Robinsion, and L. Edman, Nature Mater. **8**, 672 (2009).
[13] Q. B. Pei, G. Yu, C. Zhang, Y. Yang, and A. J. Heeger, Science **269**, 1086 (1995).
[14] D. Hohertz D and J. Gao, Adv. Mater. **20**, 3298 (2008).
[15] C. H. W. Cheng and M. C. Lonergan, J. Am. Chem. Soc. **126**, 10536 (2004).
[16] J. Fang *et al.*, J. Am. Chem. Soc. **130**, 4562 (2008).
[17] J. H. Shin *et al.*, Adv. Funct. Mater. **17**, 1807 (2007).
[18] N. D. Robinson *et al.*, Phys. Rev. B **78**, 245202 (2008).
[19] J. F. Fang, Y. L. Yang, and L. Edman, Appl. Phys. Lett. **93**, 063503 (2008).
[20] P. Matyba, M. R. Andersson, and L. Edman, Org. Electron. **9**, 699 (2008).
[21] N. D. Robinson, J. H. Shin, M. Berggren, and L. Edman, Phys. Rev. B **74**, 155210 (2006).
[22] F. Chen, *Introduction to Plasma Physics* (Plenum, New York, 1984).
[23] S. Gronenborn, B. Sturman, M. Falk, D. Haertle, and K. Buse, Phys. Rev. Lett. **101**, 116601 (2008).
[24] L.-L. Chua, J. Zaumseil, J.-F. Chang, E. Ou, P. Ho, H. Sirringhaus, and R. H. Friend, Nature (London) **434**, 194 (2005).
[25] J.-H. Shin *et al.*, Appl. Phys. Lett. **89**, 013509 (2006).